remote sensing

MDPI

Article

Strain-Rates from GPS Measurements in the Ordos Block, China: Implications for Geodynamics and Seismic Hazards

Shoubiao Zhu [1,2]

[1] National Institute of Natural Hazards, Ministry of Emergency Management of China, Beijing 100085, China; zhusb@pku.edu.cn
[2] Key Laboratory of Computational Geodynamics, Chinese Academy of Sciences, Beijing 100049, China

Abstract: A number of devastating earthquakes have occurred around the Ordos Block in recent history. For the purpose of studying where the next major event will occur surrounding the Ordos Block, much work has been done, particularly in the investigation of the Earth's surface strain rates based on GPS measurements. However, there exist striking differences between the results from different authors although they used almost the same GPS data. Therefore, we validated the method for the calculation of GPS strain rates developed by Zhu et al. (2005, 2006) and found that the method is feasible and has high precision. With this approach and the updated GPS data, we calculated the strain rates in the region around the Ordos Block. The computed results show that the total strain rates in the interior of the Block are very small, and the high values are mainly concentrated on the peripheral zones of the Ordos Block and along the large-scale active faults, such as the Haiyuan fault, which are closely aligned to the results by geological and geophysical observations. Additionally, the strain rate results demonstrated that all rifted grabens on the margin of the Ordos Block exhibit extensional deformation. Finally, based on the strain rate, seismicity, and tectonic structures, we present some areas of high earthquake risk surrounding the Ordos Block in the future, which are located on the westernmost of the Weihe Graben, both the east and westernmost of the Hetao Graben, and in the middle of the Shanxi Graben. Hence, this work is significant in contributing to a better understanding of the geodynamics and seismic hazard assessment.

Keywords: GPS data; strain rates; seismicity; ordos block; seismic hazard

Citation: Zhu, S. Strain-Rates from GPS Measurements in the Ordos Block, China: Implications for Geodynamics and Seismic Hazards. *Remote Sens.* **2022**, *14*, 779. https://doi.org/10.3390/rs14030779

Academic Editor: José Fernández

Received: 9 December 2021
Accepted: 1 February 2022
Published: 7 February 2022

1. Introduction

The Ordos Block is situated in the inner area of the Chinese Mainland. The Block is shaped like a quasi-rectangle surrounded by some faulted grabens, such as Shanxi Graben and Hetao Graben [1,2] (Zhang et al., 2003, 2006). As well, it borders Eastern Tibet in the southwest, as shown in Figure 1.

Geologically, the Ordos Block behaves strongly and stably without active tectonic faults, where earthquakes are small and rare—with magnitudes having never been over M6.0. In contrast, on the marginal area of the Ordos Block, which is full of active faults, catastrophic earthquakes took place frequently [1–5]. At the very least, six earthquakes with a magnitude $M \geq 8.0$ took place in the peripheral zone of the Ordos Block over the last 1000 years [6], causing huge disasters that affected the local residents. For example, the Huaxian earthquake, which occurred in 1556 with a magnitude of M8.5, killed over 830,000 people; the 1920 M8.0 Haiyuan earthquake caused a death toll exceeding 200,000 [7]. Thus, the peripheral zones of the Ordos are threatened by strong earthquakes. Due to the special geological features and the spatial distributions of the major earthquakes, the Ordos Block and the adjacent areas have become a hotspot for earthquake research, particularly after the 2008 Ms8.0 Wenchuan earthquake, which was located on the Eastern margin of Tibet and caused ~80,000 deaths.

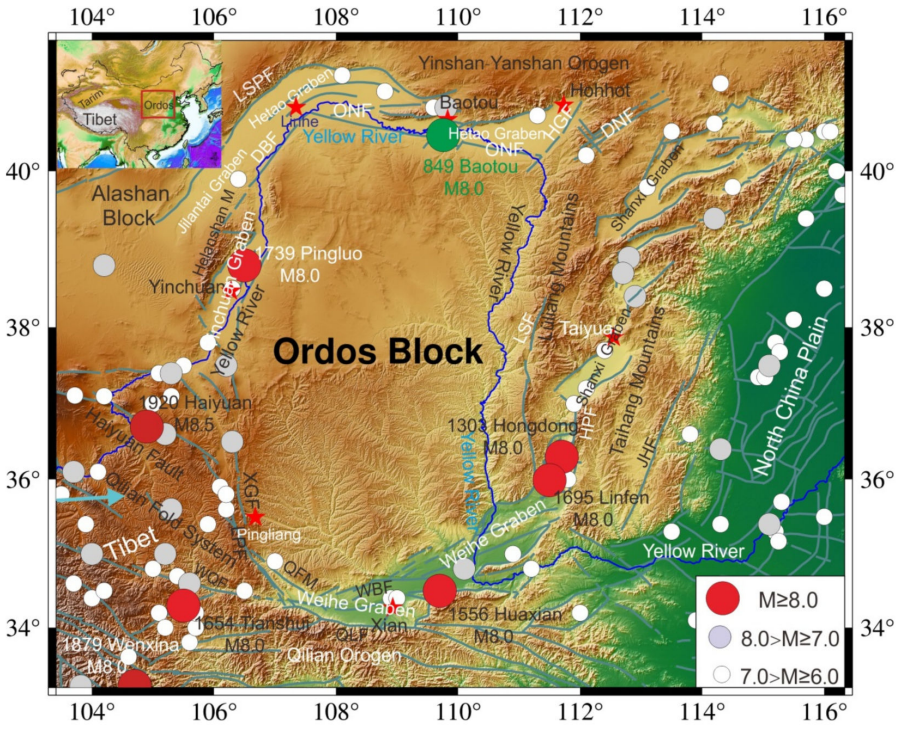

Figure 1. Geological framework and major earthquake distribution in and around the Ordos Block over the last 1000 years with magnitude M $\geq$ 6.0. In the figure, DNF, Daihai North Edge Fault; ONF, Ordos North Edge Fault; LSPF, Langshan Piedmont Fault; DBF, Dengkou-Benjing Fault; XGF, Xiaoguanshan Fault; LPF, Liupanshan Fault; QMF, Qishan-Mazhao Fault; WBF, Weihe Basin Fault; JHF, Jinhuo Fault.

Much work has been carried out in geology on the tectonic movement and ground surface deformation in the Ordos Block and its adjacent areas [1,2,4]. However, geological investigations have a long-term average, particularly in some regions in which the accuracy of the amount of tectonic movement determined by geological methods is low and/or uncertain given the influence of long-term surface erosion, weathering, and human activities. Fortunately, the GPS observation technique developed in recent decades provides an unprecedented and effective means for determining the velocity field of tectonic deformation at present. In China, since the 1990s, GPS survey has become an important tool to monitor the present crustal deformation because of its all-weather, high precision, and quasi-real time capabilities [8–14]. Moreover, different from the GPS vector, strain rates are not dependent on the coordinate system and can reveal local deformation rates and their potential links to tectonic stresses and/or seismic disaster [11,13,15–21]. Many workers in the world [10,11,13,15,16,18–29] studied how to calculate strain rates from GPS velocities. At the same time, several scientists tried to calculate the strain rates in the Chinese continent by means of many methods [9,13,15,21,25,30–33]. There is no doubt that their work gives varied approaches for obtaining the strain rate field from GPS data. However, the strain rates distributed across the Chinese continent show visible differences from each other, even though almost the same GPS velocity data were adopted by the scientists. For this reason, Zhu et al. [9,10] developed a method to calculate the strain rate based on GPS data and presented the spatial distribution of the strain rates in the Chinese Mainland [11]. The modeled results demonstrated that the method is practical and efficient in computation, and the modeled strain rates are consistent with known tectonic structures and observational geophysical data, such as the earthquake focal mechanism and stress orientations from borehole breakouts [11].

In addition, numerous authors have calculated strain rates in the Ordos Block by means of GPS velocity vector data in order to better understand the deformation mechanisms [14,17,20,34,35].

For example, with repeated GPS observations, Cui et al. [34] computed the strain rate field in the Ordos Block and presented the contour distribution of the principal strain rates in space, shown in Figure S1a. Based on almost the same GPS data as Cui et al. [34], Qu et al. [17] also calculated the strain rates using a least-squares collocation technique and presented the spatial map of the principal strain rates surrounding the Ordos Block, shown in Figure S1b. Similarly, Li et al. [20] provided the strain rate field around the Ordos Block based on almost the same GPS data, and the principal strain rates are shown in Figure S1c. Furthermore, Hao et al. [14] presented the spatial map of the principal strain rates, as shown in Figure S1d.

However, if we take a look more closely at Figure S1, it is evident that there are huge differences between them. The strain rates in these four articles are very much different from each other, although they utilized almost the same GPS velocity data. In particular, no strain rate results—as shown in Figure S1—can reflect the basic deformation pattern in the Ordos Block where little deformation occurs in the inner part and large strains are present in the peripheral zones of the Block [1,2,4,36,37]. Accordingly, Figure S1 demonstrates that large computation errors existed in their results. Given this, what are the reasonable strain rates according to GPS measurements in the Ordos Block, and, moreover, how about the seismic hazards around the Ordos Block in the future?

For this purpose, in this paper, we at first develop a new approach to verify the method by Zhu et al. [9,10]. Then, we compute the strain rates in the Ordos Block by means of the updated GPS observations [13] and compare the strain rates with other observational results, such as geological and geophysical data. Finally, we try to estimate the future seismic hazards based on the computed strain rates in and around the Ordos Block.

2. Tectonic Setting

The Ordos Block borders on the Yanshan–Yinshan Mountains, the Taihangshan Block, the Alashan Block, and the Tibetan Plateau, as shown in Figure 1. It is ~400 km from east to west, starting from within the Lüliang Mountains in the east to the Table Mountains and Yunwu Mountains in the west. It is approximately 600 km long in the NS direction, from the shore of the Yellow River in the north to the Weibei Mountains in the south, as shown in Figure 1. From a topographical perspective, the main body of the Block is the Loess Plateau above sea level, which is between 1000 m and 1700 m. On the contrary, the border of the Ordos is surrounded by several faulted basins with an average altitude of 400–1000 m. Outsides of the basins stand some high mountains, such as the Lüliang and the Taihang Mountains, the Qinling Mountains, the Helan Mountains, and the Yin Mountains (shown in Figure 1). Basins, mountains, plateaus, and active faults form the so-called "Rectangular ring" surrounding the Ordos [37].

Since the Cenozoic the Block has risen, forming a series of active tectonic faults and faulted basins. The most distinctive characteristics of the Ordos in terms of geology and geomorphology are the differentiation of the stable block, faulted basins, and lateral basin mountains. The nearly rectangular Ordos is a relatively stable and complete block in terms of long-term geological history. Almost all of the Ordos Block is surrounded by faulted basins, such as the Yinchun faulted basin, the Shanxi faulted basin, and the Weihe faulted basin—except for on the southwestern side where Eastern Tibet indents the Block. In addition, Figure 1 exhibits the main active faults all around the Ordos Block [2,36–40].

There are two special places with great significance in this tectonic framework, which are shown in Figure 1. One is situated on the southwestern edge of the Ordos, where there are no tensional faulted basins, but rather a bunch of compressive and torsion arc-shaped faults, forming the convergent boundary of the northeastern verge of Tibet. The other place is located in the northeastern corner of Ordos, which is the only region of the Ordos Block that is connected to the outside block and not disjointed by faults [37].

Above all, no earthquakes larger than or equal to M6.0 have taken place in the interior region of the Ordos and all the epicenters of major events are situated in the surrounding zone of the Block, as shown in Figure 1.

3. Data and Method

3.1. GPS Data

In order to monitor crustal deformation and try to capture some seismic precursors to be used to make earthquake predictions, China has deployed a large number of GPS observation stations in and around the Ordos Block since the 1980s. Particularly, in recent years China carried out the Crustal Movement Observation Network of China (CMONOC) Project, yielding vast amounts of GPS data. Therefore, the GPS data used in the study were mainly from CMONOC, along with local campaign GPS networks and local continuous GPS sites, respectively [13].

Wang and Shen [13] introduced the approaches to process the GPS original observational data. They also remarked that the co- and post-seismic effects of major earthquakes, such as the 2008 Wenchuan Ms8.0 and the 2011 Japan Mw9.0 earthquakes, on the ground movements in GPS observation had been removed from the GPS vectors. Thus, GPS vectors are the representative of the long-term inter-seismic movements in the Ordos Block. Figure 2 shows the GPS velocities with 70% confidence error ellipses in the Ordos Block relative to the stable Eurasia plate during the period of 1991 to 2016. From the figure, we can observe that the GPS station sites are distributed densely in space, particularly in the inner region of the Ordos Block. As a matter of fact, the GPS sites shown in the figure are the most densely distributed in space up to now. In addition, the GPS vectors suggest that the entire crustal movement of the Block is generally in the direction of the southeast with a magnitude of 5–10 mm/yr. On the whole, the figure shows that the GPS vectors in the southeast of the Ordos, including some regions of the North China Plain, are larger than those in the northwest, suggesting that there is a dominant tensile strain regime in the direction of NW-SE. However, the directions of the GPS vectors in northeastern Tibet are nearly E and NE–E, which may influence the southern part of the Ordos Block significantly. However, it is difficult for us to obtain any other information on surface deformation only from the GPS vectors. Therefore, we should calculate the strain rate field from the GPS data to discover more phenomena about earthquake physics.

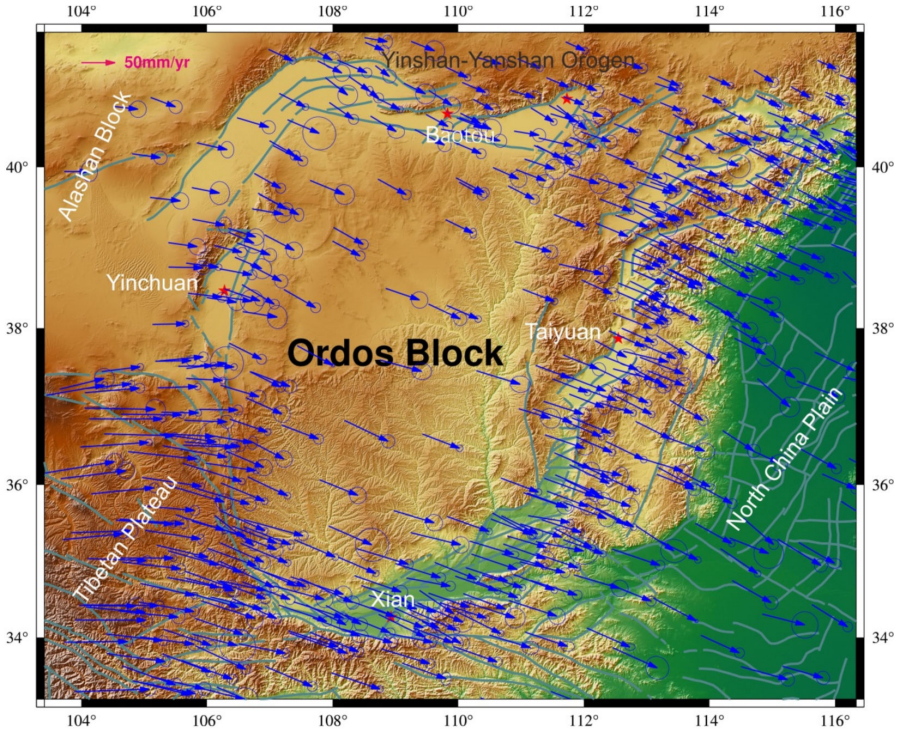

Figure 2. GPS velocities in the Ordos Block with respect to the stable Eurasian plate from 1991 to 2016 with error ellipses represented by a 70% confidence level (data from Wang and Shen [13]). The arrow stands for the movement direction of the ground surface.

3.2. Method

For the purpose of obtaining reasonable geodynamic interpretations, we should compute the strain rates from the GPS data. It seems easy and simple to compute the strain rates because it is a deterministic forward calculation. In fact, this process has been found to be much more complicated largely because the GPS sites are not regularly distributed in space. For instance, a few good Chinese workers calculated the strain rates in the Chinese Mainland utilizing different methods, but they gained different results although they used the same GPS data [9–11]. For this reason, Zhu et al. [9,10] developed a new method to calculate strain rates according to GPS data. In the approach, the kriging interpolation technology [41] was first utilized to interpolate the irregularly distributed GPS data on uniform sites, and then to compute the strain rate at each grid area, in which the strain rate is assumed to be uniform. For example, given the velocities in x- and y-directions at four nodes on the small square element, we can calculate the strain rate in the element by means of Lagrange interpolations similar to that in the finite element analysis. In order to prove the precision of this method, we will present some comparative results with real values from numerical simulation in the following section.

3.3. Validation of the Method

Since we do not know the real value of the strain/strain rate at the specific point on the Earth's surface, even though we could get the strain rate value by means of borehole surveying theoretically, we cannot directly verify the strain rates calculated from the GPS data. Thus, we do not have knowledge of which method is better and which result is correct. To this end, in this study, we will put forward an approach to verify the result of strain rates calculated from GPS vectors. The method is described in the following.

First of all, we construct a mathematical expression that randomly varies with the spatial locations. Then, the velocity vectors (or displacements) can be obtained at the sites of the GPS stations according to the mathematical expression that has been constructed. At last, we could compute the strain rate at each site in space, according to the components of the partial derivatives, to the constructed function. In this way, the strain rate at each site in space is a true value with an error of zero because the value is derived directly by means of purely mathematical operations. The strain rate is called a true strain, or true strain rate (TSR), in the following context.

On the other hand, we could calculate the strain rate (CSR) with the method developed by Zhu et al. [9,10]—or some of the other authors—with the data of velocity vectors derived from the mathematical operation above. By comparing CSR with TSR, we can judge how well the method is.

Here, suppose velocities on the Earth's surface in θ- and φ-direction (east- and north-direction in a spherical coordinate system) are varied according to the following function.

$$\begin{cases} v_\theta = \mathrm{f}_u(\theta, \varphi) \\ v_\varphi = \mathrm{f}_v(\theta, \varphi) \end{cases} \tag{1}$$

Then, the components of strain rates on the spherical Earth's surface can be expressed as [42],

$$\begin{cases} \dot{\varepsilon}_\theta = \frac{1}{R} \cdot \frac{\partial v_\theta}{\partial \theta} \\ \dot{\varepsilon}_\varphi = \frac{1}{R \sin\theta} \cdot \frac{\partial v_\varphi}{\partial \varphi} + \frac{v_\theta}{R} ctg\theta \\ \dot{\varepsilon}_{\theta\varphi} = \frac{1}{2}[\frac{1}{R}(\frac{\partial v_\varphi}{\partial \theta} - v ctg\theta) + \frac{1}{R \sin\theta} \cdot \frac{\partial v_\theta}{\partial \varphi}] \end{cases} \tag{2}$$

where R denotes the Earth's radius.

Therefore, principal strain rates could be obtained based upon equation set (2) [43].

$$\dot{\varepsilon}_{1,2} = \frac{\dot{\varepsilon}_\theta + \dot{\varepsilon}_\varphi}{2} \pm \sqrt{\frac{(\dot{\varepsilon}_\theta - \dot{\varepsilon}_\varphi)^2}{4} + \dot{\varepsilon}_{\theta\varphi}{}^2} \tag{3}$$

where $\dot{\varepsilon}_{1,2}$ represents two principal strain rates—one is maximum, the other is minimum.

Likewise, the maximum shear strain rate and the second invariant of strain rate (SR) can be expressed as (4) and (5), respectively.

$$\dot{\chi} = (\dot{\varepsilon}_1 - \dot{\varepsilon}_2)/2 \tag{4}$$

$$SR = \sqrt{\dot{\varepsilon}_\theta{}^2 + \dot{\varepsilon}_\varphi{}^2 + 2\dot{\varepsilon}^2{}_{\theta\varphi}} \tag{5}$$

In an actual simulation, Equation (1) can be taken into many forms. In general, Equation (1) is taken as a periodic function in space. For example, in this study, we specify the functions as

$$\begin{cases} v_\theta = -2\sin(20(\theta + 20.0^0)) + 3\cos(8\varphi) \\ v_\varphi = 3\sin(18(\theta + 10.0^0)) - 2\cos(10\varphi) \end{cases} \tag{6}$$

where v_θ and v_φ are surface velocities in north- and east-directions, respectively, with the dimension of mm/yr. θ stands for co-latitude and φ represents longitude in degrees.

According to Equation (6), we could generate velocity vectors at the points where the GPS stations were deployed in and around the Ordos Block, as in Figure 2. Then, based on the above procedures, the strain rates will be calculated by Equations (1)–(6) and by the method developed by Zhu et al. [9,10], respectively. The corresponding principal strain rates are plotted in Figure 3. In Figure 3a, the real values of the strain rates are shown, and the computed ones are displayed in Figure 3b. By examining Figure 3a,b in detail, we could clearly see that the computed strain rates match the true values very well. In addition, we chose many other expressions of Equation (6) and the varied parameters, and repeated computations of the strain rates based on the above procedures. We found that the strain rates computed by the method developed by Zhu et al. [9,10] are in good agreement with the true strain rates in any case.

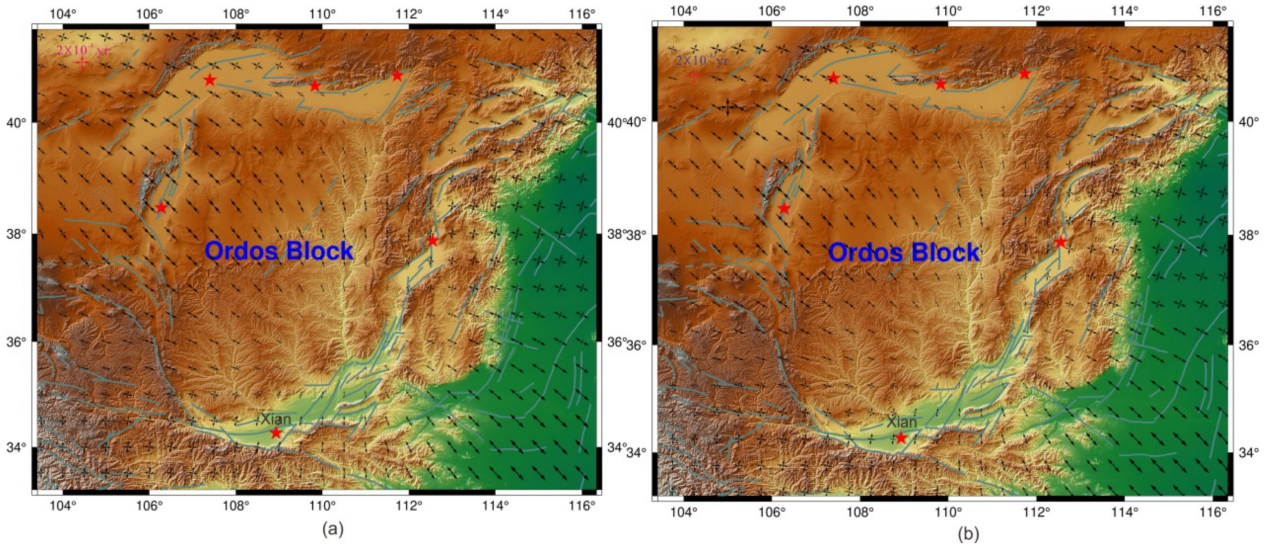

Figure 3. Comparing the real strain rates with the computed counterparts based on the same data. (**a**) Distribution map of principal strain rates calculated mathematically based on the Equations (1)–(6); (**b**) Computed principal strain rates with the method developed by Zhu et al. [9,10].

However, from the viewpoint of mathematics, the above verification is not complete and needs further research. Nevertheless, through digital verifications we could understand that Zhu's approach is reasonable and accurate in the calculation of strain rates based on real GPS measurements.

4. Strain Rate Results

Figure 4 displays the distribution of horizontal principal strain rates in the Ordos Block. Obviously, it highlights that the principal strain rates in the inner region of the Block are very small, and the large values are mostly concentrated on the verge of the Ordos and along the large-scale faults, such as the Haiyuan fault, which is generally in agreement with the results by other works [11,13].

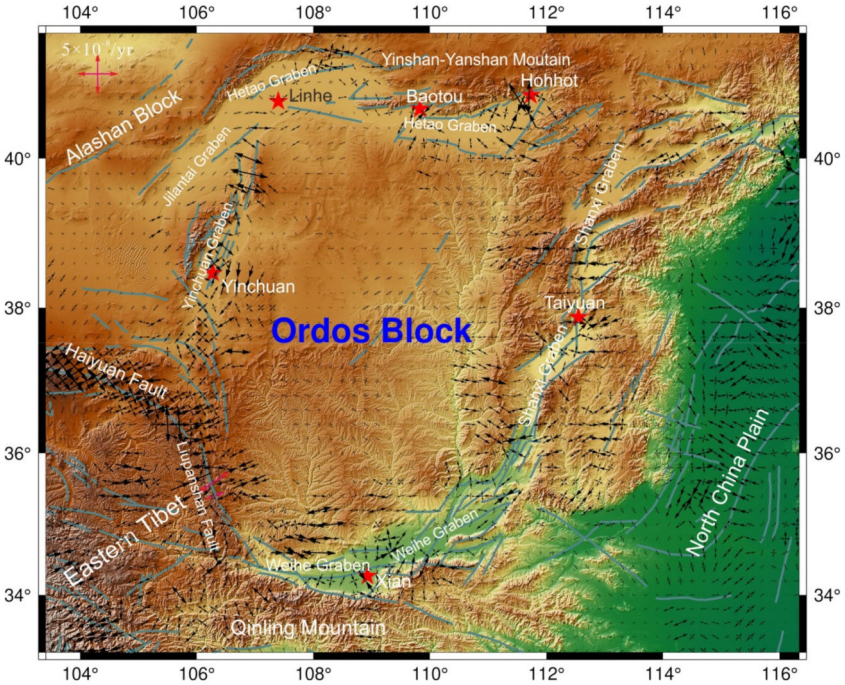

Figure 4. Spatial distribution of principal strain rates in the Ordos Block with grid size of 0.25° × 0.25° (the arrow outward stands for tensile, and the inward represents compressive). The red arrows suggest the tensile deformation in compressive environment.

On the whole, the principal strain rates are compressive in the NE-SW and are extensive in the NW-SE directions in the Ordos Block, which is consistent with the stress regime from geological investigations [1,2,4,36,37] and stress surveys [44]—even though their orientations are different in different areas. In the main collision zones between Eastern Tibet and the southwest of the Ordos, the principal compressive strain rates are found to be the highest value of 3~5 $\times$ 10^{-8}/yr trending in the NW direction, which is consistent with the convergence direction between Eastern Tibet and the Ordos. Along the Haiyuan fault, the figure shows that the magnitudes of the maximum and minimum principal strain rates are almost the same with the angle between the maximum compressive principal strain rates and the fault trace being 45°, implying the dominant strike-slip sense of fault mechanism.

In the Yinchuan Graben, located on the western verge of the Ordos Block, together with both the north and south of the Graben, we found extensive deformation with an orientation of nearly W–E. However, to the east of the Graben, compressive strain rates are seen trending N–S with the value of 2~4 $\times$ 10^{-8}/yr. We should note that the 1739 M8.0 Pingluo earthquake took place in the Yingchuan Graben, which was the largest event ever documented in the Graben [45]. Considering the complexity of the present strain rates from GPS measurements, the Yinchuan Graben and adjacent areas could be prone to major earthquakes in the future.

The strain rates in the Hetao Graben, located on the northern verge of the Ordos Block, are found to be extensive from the western corner to the easternmost end generally. The largest value of extensive strain rates is found around the south of the Hohhot, which is the easternmost part of the Hetao Graben, where no large earthquakes have occurred for

a long time. The largest earthquake that ever occurred in the Hetao Graben was the M8.0 Baotou earthquake in A. D. 849, shown in Figure 1. Thus, the eastern region of the Hetao Graben is also regarded as an earthquake-prone region.

The tensile strain rates are also found in the Shanxi Graben and the Lüliang Mountains, east of the Ordos Block. In addition, large earthquakes occurred frequently along the Shanxi Graben. Especially, in this area, two major M8.0 earthquakes occurred in Hongdong and Linfen in 1303 and in 1695, respectively [46,47]. The two major earthquakes are only 40 km apart in space and 392 years apart in time. Given this, will any major earthquake come here again in the future? This question will be of great concern in the field of earthquake science.

The southern brink of the Ordos Block is the Weihe Graben where the principal strain rates present as tensile overall in the directions of nearly W–E, possibly because the Qinling Mountains move faster than the southern Ordos, as observed from the GPS velocities displayed in Figure 2. It is worth emphasizing that the 1556 M8.5 Huaxian earthquake took place on the southeast border of the Weihe Graben, which killed over 830,000 people [48]. Since then, there have been no major earthquakes. Thus, the Weihe Graben is one of the most hazardous zones for future major earthquakes.

Furthermore, in Figure 4 it is shown that in the convergence zone there is extensional deformation that appears around the Liupanshan thrust fault, with the arrows for the principal strain rates indicated by the red colors in Figure 5. This unexpected phenomenon has not yet been uncovered by any other previous works and is only based on GPS measurements [13,14,17,20,34,35]. The mechanism for this phenomenon is interpreted graphically in Figure 5. The southern segment of the Liupanshan fault consists of two strands, one is called the east Liupanshan thrust fault and the other is the west Liupanshan back-thrust fault [49,50]. The figure shows that the extensional deformation could be exhibited in the middle of the east and west Liupanshan faults, although the whole Liupanshan faults, on the northeastern verge of the Tibetan plateau, is in a compressive environment.

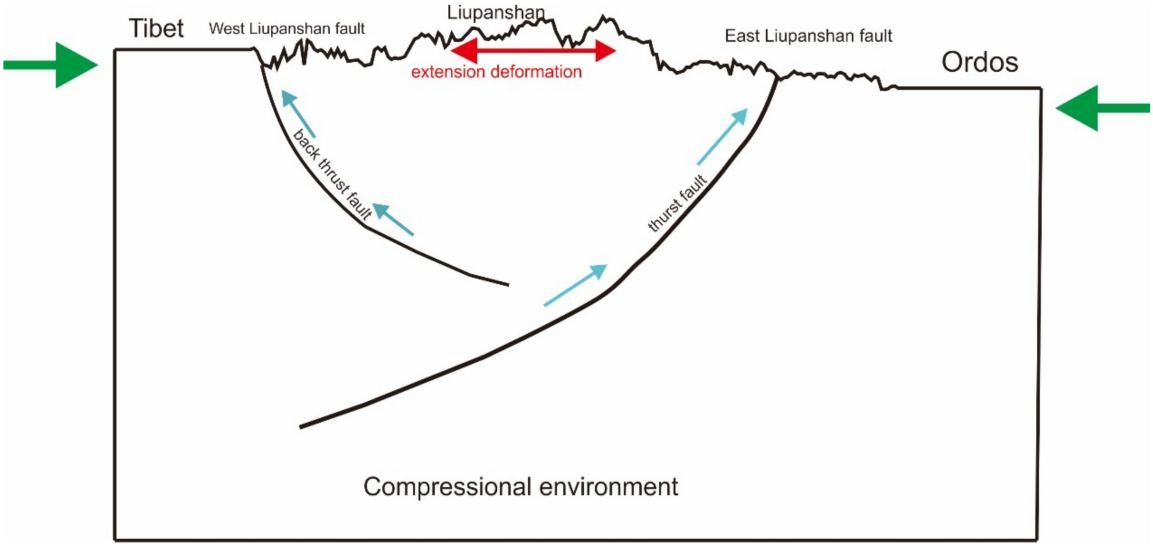

Figure 5. Sketch map for explaining the mechanism of the extensional deformation under the compressive stress environment. The east Lipanshan fault is a thrust fault dipping SW, while the west Liupanshan fault is a back-thrust fault dipping NE.

Figure 6 depicts the spatial contour map of the maximum shear strain rates. In the figure, we can observe that the large magnitudes of the maximum shear strain rates are located around the edge of the Block, and the lower ones are found in the inner region of the Ordos Block, which is consistent with our general knowledge about the deformation of the Ordos Block in geology. In reality, when we examine the figure in more detail, we can observe that the largest magnitudes of the maximum shear strain rates are focused in a few areas, such as the Haiyuan fault zone, the Yinchuan Graben, west of the Xian City

in the Weihe Graben, and south of the Hohhot in the Hetao Graben, respectively—with a magnitude of 3–4 $\times$ 10^{-8}/yr.

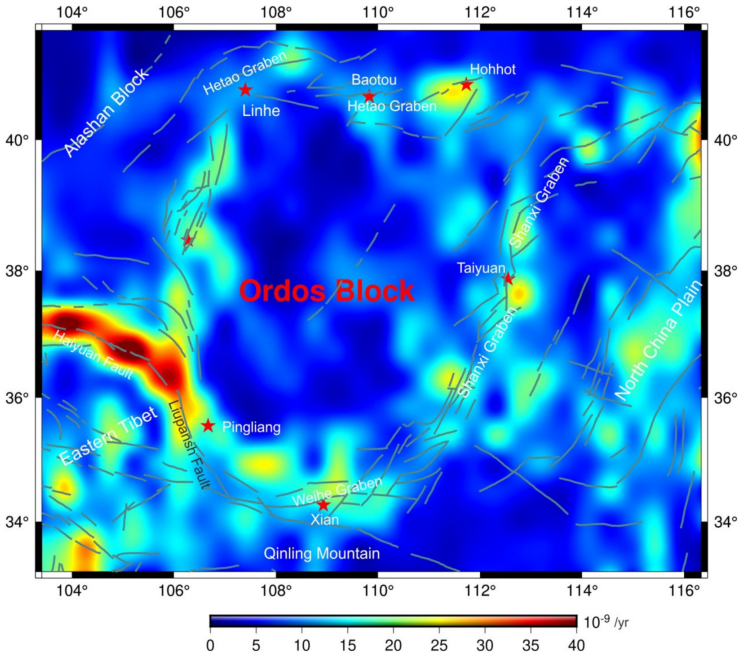

Figure 6. The spatial contour map of the maximum shear strain rates in the Ordos Block.

The spatial distribution of the second invariant of strain rate (SR), which reflects the magnitude of the total strain rates, is depicted in Figure 7. When we compare Figure 7 with Figure 6, we can see that there are some differences between them, although the basic pattern is almost the same. Similar to the contour map of the maximum shear strain rates, the high value of the SR is largely distributed along the Haiyuan fault and on the verge of the Ordos Block. In addition, we notice that the SR is heterogeneously distributed around the Ordos Block.

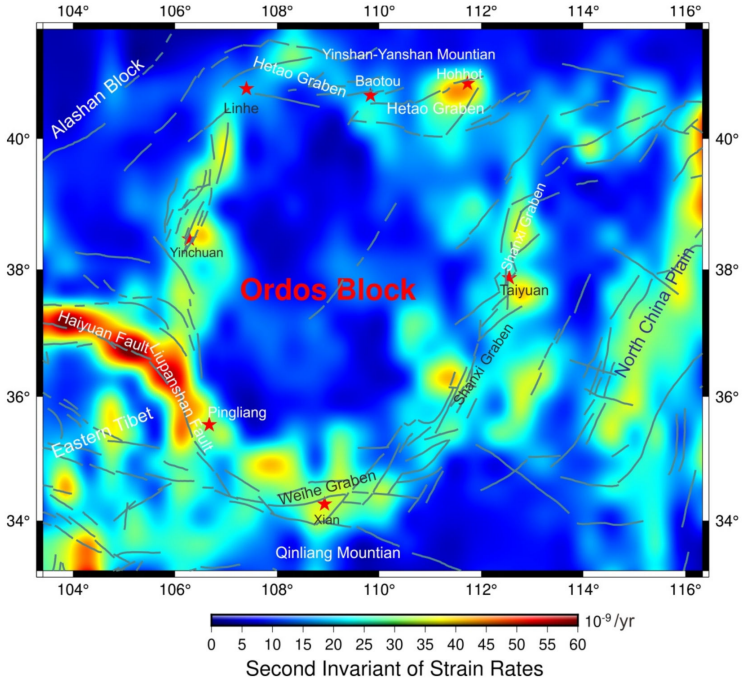

Figure 7. The spatial contour map of the second invariants of strain rate tensors (SR) in and around the Ordos Block.

5. Discussions

5.1. Comparison of the Strain Rates with Others

Previous works [13,14,17,20,34,35] that used different approaches to study strain rates and tectonic movements in the peripheral regions of the Ordos Block have presented useful clues to the geodynamics in the study area. However, their results for the strain rates in the Ordos Block exhibit huge differences from each other, and deviated from the basic pattern of real deformation, in which strain rates are small in the interior and large on the verge of the Block.

Figure S1a shows that the principal strain rates from Cui et al. [34] are obviously larger in the inner part of the Ordos than those in the Weihe Graben, which is in the southern side of the Block. In Figure S1b, the principal strain rates in most inner regions of the Ordos Block are much greater than those in the northwestern area of the Hetao Graben and are almost at the same level as those in the Weihe Graben and Shanxi Graben [17]. What is more, the strain rates in the interior part of the Block are larger than those in the Shanxi and Weihe Graben [20], as shown in Figure S1c. More than that, within the area (Longitude: 107°–115°; Latitude: 33°~42°), which surrounds the whole Ordos Block, the largest principal strain rate is located in the center region of the Ordos Block, displayed in Figure S1d [14]. In addition, these authors did not uncover the tensile deformation between the east and west Liupanshan thrust faults, shown in Figure 4.

Therefore, the above results for the strain rates from the previous authors did not reflect the basic deformation feature of the Ordos Block. The reason for this is complex, but it is mainly due to the different approaches they utilized and the irregular distribution of GPS observational sites—given that they are dense in one region and quite sparse in other areas [11]. Additionally, I found that the methods they used were generally based on least square principles, possibly causing significant errors in the processing of the irregularly distributed GPS vectors. On the contrary, the approach proposed by Zhu et al. [9,10] made use of the Krige technique, which was specially proposed to deal with irregularly scattered discrete observational data in space [41]. Therefore, it is an optimal choice for one to interpolate the GPS velocity data on grids by means of the kriging method. Based on the verification above, we found that Zhu's method is practical and has high accuracy, which can be extended to other places.

However, we should note that the spatial distribution of strain rates calculated from the GPS velocities would be affected if noises or some other uncertainties are present in the GPS measurements. The use of fuzzy data analysis techniques may be required for this case [51], which will be studied in depth in the future.

Overall, the directions of the principal strain rates in the paper are consistent with those of the observational principal stresses [44]. The orientation of the predominant compressive principal strain rates in the Ordos Block is in the direction of NE–SW, and the predominant tensile strain rates are trending toward NW–SE.

5.2. Implications for Geodynamics and Seismic Hazard

The relationship between Earth's surface deformation and seismicity is complicated. Most interestingly, there are two completely opposite opinions. The first view thought that higher strain rates are generally associated with larger or more frequent earthquakes [11,17,21,52–55]. For example, strain rates are larger in western China than those in eastern China; correspondingly, the major earthquakes more frequently occurred in western China than in eastern China [11]. Similarly, the strain rates are larger in the peripheral region of the Ordos Block than those in the interior region of the Block, leading to few earthquakes that have occurred in the inner part of the Block and major events having often occurred in the surrounding area of the Ordos. In contrast, the other view assumed that higher strain rates are generally related to low seismicity, and strong events that frequently occurred in the region had a small deformation [56,57]. For instance, Riguzzi et al. [57] found that larger earthquakes ($M > 4.0$) occurred with larger probability in regions of smaller strain rates in Italy by means of comparison of the seismicity and total strain rates. Doglioni et al. [56]

presented the evidence that earthquakes are produced along fault segments with small strain rates relative to the bordering larger strain rate regions before earthquakes in tensile, compressive, and strike-slip tectonic backgrounds. In fact, as early as in 1973, Guo et al. (1973) pointed out that an earthquake would often occur along the stress accumulation unit (assumed as seismic focus) where the rock is strong and deformation is small, while the stress adjustment unit, in which the rock medium is soft and broken and deformation is large, transmits the elastic energy to the stress accumulation unit. Thus, it can be seen that the viewpoint of Doglioni et al. [56] is similar to the idea of Guo et al. [58]. Particularly, we should be clear that the 2008 Ms8.0 Wenchuan, China earthquake took place on the Longmen Shan fault zone where the Earth's surface deformation was small based on GPS measurement and geological investigations [59,60]. Additionally, both events in Italy—one is the 2009 L'Aquila (ML = 5.9) earthquake and the other the 2012 Emilia earthquake (ML = 5.9)—took place in areas of small SR that were close to areas of large SR [57].

The above opposite perspectives on surface deformation and earthquakes are two end members. In my opinion, the former is reasonable for the large scale and the latter is in line with reality for the small scale of an earthquake focal source. As to the relationship between deformation and seismicity in the Ordos Block, we adopted a strategy of learning from the strong points of the above two end members. Based on previous work, we estimated that the most likely locations for future major earthquakes are based on the principle that large earthquakes will occur along existing large active faults with lower SR, where the fault is locked with high friction and is located close to higher strain rates, in which the friction is low and the velocity strengthening could not accumulate enough energy for major earthquakes.

Figure 8 displays the most likely locations for future major earthquakes surrounding the Ordos. The figure shows there are four earthquake-prone locations marked by white circles with capital letters from A1 to A4.

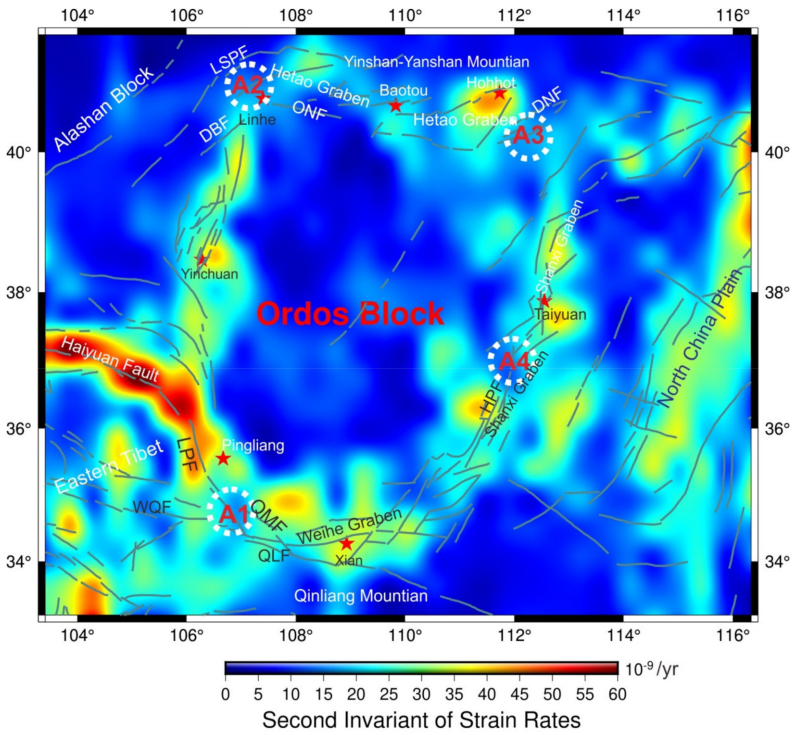

Figure 8. Spatial distribution of SR and the most likely regions for future major earthquakes represented by A1, A2, A3, and A4 with dashed circles. In the figure, DNF, Daihai North Edge Fault; ONF, Ordos North Edge Fault; QMF, Qishan-Mazhao Fault; QLF, Qinling Fault; DBF, Dengkou-Benjing Fault; LSPF, Langshan Piedmont Fault; HPF, Huoshan Piedmont Fault; WQF, Western Qinliang Fault.

A1 is located on the westernmost part of the Weihe Graben with low SR. However, around the A1, SR is high. Also, some active faults, such as the Liupanshan fault and Qishan–Mazhao fault intersect at A1. In addition, there have been no earthquakes that have occurred on A1 with a magnitude over 7.0 in the last 1000 years.

A2 is situated in the western part of the Hetao Graben, on the northwestern corner of the Block, where SR is low. In addition, numerous active faults pass through A2, such as the Langshan piedmont fault [61] and the Ordos north edge fault. The latest earthquake event may have been Mw ~ 7.8, and probably occurred within the past ~1880 yrs, with an average recurrence interval of 2450 yrs [40]. Hence, the probability of a major earthquake along the Langshan piedmont fault is high. Additionally, A2 encircles Linhe City (now renamed as Bayannuoer City) where the land is fertile and densely populated. Once a strong or major earthquake occurs, the seismic hazard will be much more severe.

A3 is the other region with low SR, bordered by high SR, as shown in Figure 8, and is situated on the northeast corner of the Block and is also on the eastern end of Hetao Graben, to the southeast of Hohhot, which is the capital city of Inner Mongolia, China. Also, A3 is the intersection region between the Ordos North Edge fault, Daihai fault, and Horinger fualt. Moreover, A3 is near the epicenter of the 869 Baotou earthquake (M = 8.0). Thus, taken together, A3 is considered to be the other possible region for a future major earthquake.

A4 is located on the middle part of the Shanxi Graben in the eastern brink of the Ordos, in which the Huoshan piedmont fault [62], Taigu fault, and Jiaocheng fault intersect. Particularly, two major earthquakes (M = 8.0), the 1303 Hongdong event and the 1695 Linfen earthquake, are located within 100 km of each other in the south. In addition, in the last 300 years, no earthquake of magnitude 7 or greater has occurred. It can be seen that A4 is one of the most likely areas for future major earthquakes.

6. Conclusions

We validated the method for the calculation of strain rates with GPS data that was developed by Zhu et al. [9,10], and found that the method is reasonable and practical in computing strain rates.

The calculated results show that the principal strain rates in the inner region of the Ordos Block are very small, and the high strain rates are mainly concentrated on the peripheral zones of the Block and along the large-scale faults, such as the Haiyuan fault, which is consistent with the results from the geophysical and geological surveys. Overall, the principal strain rates are characterized by NE–SW compression and NW–SE extension around the Ordos Block, which is in good agreement with the stress regime from the geological investigations and stress measurements.

Based on SR, seismicity, and tectonic structures, the most earthquake-prone regions surrounding the Ordos are presented. These areas are situated on the westernmost part of the Weihe Graben that borders on the south of the Block, on the west and easternmost part of the Hetao Graben, and in the middle part of the Shanxi Graben, which is on the eastern verge of the Ordos. We should pay more attention to these areas by means of intensified monitoring and in-depth research.

Supplementary Materials: The following supporting information can be downloaded at: https://www.mdpi.com/article/10.3390/rs14030779/s1, Figure S1: Comparison of different principal strain rates from different authors based on almost the same GPS data. (a) Principal strain rates computed by Cui et al., 2016 [34] (in Figure 3); (b) Principal strain rates by Qu et al., 2017 [7] (in Figure 7); (c) Principal strain rates by Li et al., 2018 [20] (in Figure 5); (d) Principal strain rates by Hao et al., 2021 [14] (in Figure 3b).

Funding: This research was funded by National Natural Science Foundation of China (41874060, 41574041), National Key Research and Development Program of China (2017YFC1500104), and by the Research Grant from National Institute of Natural Hazards, MEMC (ZDJ2020-15).

Institutional Review Board Statement: Not applicable.

Informed Consent Statement: Not applicable.

Data Availability Statement: All the GPS data used in the current study are available from Wang and Shen (2020), and all earthquake data are from National Earthquake Data Center of China (downloaded from: https://data.earthquake.cn/gcywfl/index.html). All websites were last accessed on 31 May 2021. The supplemental material for this paper includes strain rate figures based on GPS data (Cui et al., 2016; Qu et al., 2017; Li et al., 2018; Hao et al., 2021).

Acknowledgments: I thank three anonymous reviewers and the Editor who contributed significantly to improving the quality of the original paper. This work was jointly supported by National Natural Science Foundation of China (41874060, 41574041), National Key Research and Development Program of China (2017YFC1500104), and by the Research Grant from National Institute of Natural Hazards, MEMC (ZDJ2020-15).

Conflicts of Interest: The author declares no conflict of interest relevant to this study.

References

1. Zhang, P.; Deng, Q.; Zhang, G.; Ma, J.; Gan, W.; Min, W.; Mao, F.; Wang, Q. Active tectonic blocks and strong earthquakes in the continent of China. *Sci. China Ser. D Earth Sci.* **2003**, *46*, 13–24.
2. Zhang, Y.Q.; Liao, C.Z.; Shi, W.; Hu, B. Neotectonic evolution of the peripheral zones of the Ordos Basin and geodynamic setting. *Geol. J. China Univ.* **2006**, *12*, 285–297.
3. Deng, Q.; Sung, F.; Zhu, S.; Li, M.; Wang, T.; Zhang, W.; Burchfiel, B.C.; Molnar, P.; Zhang, P. Active faulting and tectonics of the Ningxia-Hui autonomous region, China. *J. Geophys. Res.* **1984**, *89*, 4427–4445.
4. Deng, Q.D.; Cheng, S.P.; Min, W. Discussion on Cenozoic tectonics and dynamics of Ordos Block. *J. Geomech.* **1999**, *5*, 20–26.
5. Deng, Q.; Liao, Y. Paleoseismology along the range-front fault of Helan Mountains, north central China. *J. Geophys. Res. Solid Earth* **1996**, *101*, 5873–5893. [CrossRef]
6. Wang, C.Y.; Sandvol, E.; Zhu, L.; Lou, H.; Yao, Z.; Luo, X. Lateral variation of crustal structure in the Ordos Block and surrounding regions, North China, and its tectonic implications. *Earth Planet. Sci. Lett.* **2014**, *387*, 198–211. [CrossRef]
7. Qu, W.; Lu, Z.; Zhang, M.; Zhang, Q.; Wang, Q.; Zhu, W.; Qu, F. Crustal strain fields in the surrounding areas of the Ordos Block, central China, estimated by the least-squares collocation technique. *J. Geodyn.* **2017**, *106*, 1–11. [CrossRef]
8. Ma, Z.; Chen, X.; Ye, S.; Lai, X.; Wei, Z.; Chen, J.; Ning, J.; Xu, H.; Ding, G. Contemporary crustal movement of continental China obtained by Global Positioning System (GPS) measurements. *Chin. Sci. Bull.* **2001**, *46*, 1552–1554. [CrossRef]
9. Zhu, S.B.; Cai, Y.E.; Shi, Y.L. Computation of the present-day strain rate field of the Qinghai-Tibetan plateau and its geodynamic implications. *Chin. J. Geophys.* **2005**, *48*, 1053–1061. [CrossRef]
10. Zhu, S.; Cai, Y.; Shi, Y. The contemporary tectonic strain rate field of continental China predicted from GPS measurements and its geodynamic implications. *Pure Appl. Geophys.* **2006**, *163*, 1477–1493. [CrossRef]
11. Zhu, S.; Shi, Y. Estimation of GPS strain rate and its error analysis in the Chinese continent. *J. Asian Earth Sci.* **2011**, *40*, 351–362. [CrossRef]
12. Wang, Q.; Zhang, P.Z.; Freymueller, J.T.; Bilham, R.; Larson, K.M.; You, X.; Niu, Z.; Wu, J.; Xi, Y.; Liu, J. Present-day crustal deformation in China constrained by global positioning system measurements. *Science* **2001**, *294*, 574–577. [CrossRef] [PubMed]
13. Wang, M.; Shen, Z.K. Present-day crustal deformation of continental China derived from GPS and its tectonic implications. *J. Geophys. Res. Solid Earth* **2020**, *125*, e2019JB018774. [CrossRef]
14. Hao, M.; Wang, Q.; Zhang, P.; Li, Z.; Li, Y.; Zhuang, W. "Frame wobbling" causing crustal deformation around the Ordos Block. *Geophys. Res. Lett.* **2021**, *48*, e2020GL091008. [CrossRef]
15. Allmendinger, R.W.; Reilinger, R.; Loveless, J. Strain and rotation rate from GPS in Tibet, Anatolia, and the Altiplano. *Tectonics* **2007**, *26*, TC3013. [CrossRef]
16. Bennett, R.A.; Wernicke, B.P.; Niemi, N.A.; Friedrich, A.M.; Davis, J.L. Contemporary strain rates in the northern Basin and Range province from GPS data. *Tectonics* **2003**, *22*, TC001355. [CrossRef]
17. Ward, S.N. Methods for evaluating earthquake potential and likelihood in and around California. *Seismol. Res. Lett.* **2007**, *78*, 121–133. [CrossRef]
18. Kreemer, C.; Blewitt, G.; Klein, E.C. A geodetic plate motion and Global Strain Rate Model. *Geochem. Geophys. Geosystems* **2014**, *15*, 3849–3889. [CrossRef]
19. Zheng, G.; Wang, H.; Wright, T.J.; Lou, Y.; Zhang, R.; Zhang, W.; Shi, C.; Huang, J.; Wei, N. Crustal deformation in the India-Eurasia collision zone from 25 years of GPS measurements. *J. Geophys. Res. Solid Earth* **2017**, *122*, 9290–9312. [CrossRef]
20. Li, S.; Li, C.; Zhou, Q. Kinematic analysis of the Ordos Block and surrounding area based on GPS data: An initiative–passive vortex structure model. *Arab. J. Geosci.* **2018**, *11*, 627. [CrossRef]
21. Rui, X.; Stamps, D.S. A geodetic strain rate and tectonic velocity model for China. *Geochem. Geophys. Geosystems* **2019**, *20*, 1280–1297. [CrossRef]
22. Kato, T.; El-Fiky, G.; Oware, E. Crustal strains in the Japanese islands as deduced from dense GPS array. *Geophys. Res. Lett.* **1998**, *25*, 3445–3448. [CrossRef]
23. Kahle, H.G.; Cocard, M.; Peter, Y.; Geiger, A.; Reilinger, R.; McClusky, S.; King, R.; Barka, A.; Veis, G. The GPS strain rate field in the Aegean Sea and western Anatolia. *Geophys. Res. Lett.* **1999**, *26*, 2513–2516. [CrossRef]

24. Calais, E.; Galisson, L.; Stephan, J.; Delteil, J.; Deverchere, J.; Larroque, C.; Mercier de Lepinay, B.; Popoff, M.; Sosson, M. Crustal strain in the Southern Alps, France, 1948–1998. *Tectonophysics* **2000**, *319*, 1–17. [CrossRef]
25. Holt, W.; Chamot-Rooke, N.; Pichon, X.L.; Haines, A.J.; Shen-Tu, B.; Ren, J. Velocity field in Asia inferred from Quaternary fault slip rates and Global Positioning System observations. *J. Geophys. Res.* **2000**, *105*, 19185–19210. [CrossRef]
26. Henry, P.; Mazzotti, S.; Pichon, L. Transient and permanent deformation of central Japan estimated by GPS: 1. Interseismic loading and subduction kinematics. *Earth Planet. Sci. Lett.* **2001**, *184*, 443–453. [CrossRef]
27. Savage, J.C.; Gan, W.; Svarc, J.L. Strain accumulation and rotation in the Eastern California Shear Zone. *J. Geophys. Res.* **2001**, *106*, 21995–22007. [CrossRef]
28. Mazzotti, S.; James, T.S.; Henton, J.; Adams, J. GPS crustal strain, postglacial rebound, and seismic hazard in eastern North America: The Saint Lawrence valley example. *J. Geophys. Res.* **2005**, *110*, B11301. [CrossRef]
29. Lukhnev, A.V.; San'kov, V.A.; Miroshnichenko, A.I.; Ashurkov, S.V.; Calais, E. GPS rotation and strain rates in the Baikal–Mongolia region. *Russ. Geol. Geophys.* **2010**, *51*, 785–793. [CrossRef]
30. Shen, Z.; Wang, M.; Gan, W.; Zhang, Z. Contemporary tectonic strain rate field of Chinese Continent and its geodynamic implications. *Earth Sci. Front.* **2003**, *10*, 93–100.
31. Jiang, Z.; Ma, Z.; Zhang, X.; Wang, Q.; Wang, S. Horizontal strain field and tectonic deformation of the China Mainland inferred from GPS measurements. *Chin. J. Geophys.* **2003**, *46*, 352–358. [CrossRef]
32. Li, Y.; Li, Z.; Zhang, J.; Huang, C.; Zhu, W.; Wang, W.; Guo, L.; Zhang, Z.; Yang, C. Horizontal strain field in the Chinese mainland and its surrounding areas. *Chin. J. Geophys.* **2004**, *47*, 245–257. [CrossRef]
33. Gan, W.; Zhang, P.; Shen, Z.; Niu, Z.; Wang, M.; Wan, Y.; Zhou, D.; Cheng, J. Present-day crustal motion within the Tibetan Plateau inferred from GPS measurements. *J. Geophys. Res.* **2007**, *112*, B08416. [CrossRef]
34. Cui, D.; Hao, M.; Li, Y.; Wang, W.; Qin, S.; Li, C. Present-day crustal movement and strain of the surrounding area of Ordos Block derived from repeated GPS observations. *Chin. J. Geophys.* **2016**, *59*, 3646–3661. (In Chinese with an English abstract)
35. Middleton, T.A.; Parsons, B.; Walker, R.T. Comparison of seismic and geodetic strain rates at the margins of the Ordos Plateau, northern China. *Geophys. J. Int.* **2018**, *212*, 988–1009. [CrossRef]
36. Shi, W.; Dong, S.; Hu, J. Neotectonics around the Ordos Block, North China: A review and new insights. *Earth Sci. Rev.* **2020**, *200*, 102969. [CrossRef]
37. The research group on "Active fault system around Ordos massif"; State Seimological Bereau. *Active Fault System around Ordos Massif*; Seimological Press: Beijing, China, 1988.
38. Wang, J. A study on the tectonics of the Weihe river graben. *Geol. Rev.* **1984**, *30*, 217–223.
39. Rao, G.; Lin, A.; Yan, B. Paleoseismic study on active normal faults in the southeastern Weihe Graben, central China. *J. Asian Earth Sci.* **2015**, *114*, 212–225. [CrossRef]
40. Rao, G.; Chen, P.; Hu, J.; Yu, Y.; Qiu, J. Timing of Holocene paleo-earthquakes along the Langshan Piedmont Fault in the western Hetao Graben, North China: Implications for seismic risk. *Tectonophysics* **2016**, *677*, 115–124. [CrossRef]
41. Deutsch, C.V.; Journel, A.G. *GSLIB: Geostatistical Software Library and User's Guide*, 2nd ed.; Oxford University Press: New York, NY, USA, 1997.
42. Love, A.E.H. *A Treatise on the Mathematical Theory of Elasticity*, 4th ed.; Cambridge University Press: Dover, UK; Cambridge University Press: Mineola, NY, USA, 1944.
43. Turcotte, D.L.; Schubert, D. *Geodynamics*, 2nd ed.; Cambridge University Press: Cambridge, UK, 2002.
44. Hu, X.; Zang, A.; Heidbach, O.; Cui, X.; Xie, F.; Chen, J. Crustal stress pattern in china and its adjacent areas. *J. Asian Earth Sci.* **2017**, *149*, 20–28. [CrossRef]
45. Lei, Q.Y.; Chai, C.Z.; Du, P.; Yu, J.X.; Wang, Y.; Xie, X.F. The seismogenic structure of the M8. 0 Pingluo earthquake in 1739. *Seismol. Geol.* **2015**, *37*, 413–429. (In Chinese with an English abstract)
46. Qin, B.; Yan, W. Study on the cause of the 1695 M8 Linfen great earthquake. *J. Catastrophol.* **1992**, *7*, 14–18. (In Chinese with an English abstract)
47. Qi, Y.; Lu, G.; Sun, L.; Fang, S.; Wang, X.; Feng, X.; Diao, G. Seismogenic Fault of the 1303 Hongdong M8 Earthquake in Shanxi Province. *Earthquake* **2017**, *31*, 148–157. (In Chinese with an English abstract)
48. Ma, J.; Feng, X.J.; Li, G.Y.; Li, X.; Zhang, Y. The coseismic vertical displacements of surface rupture zone of the 1556 Huaxian earthquake. *Seismol. Geol.* **2016**, *38*, 22–30.
49. Su, X.; Yao, L.; Wu, W.; Meng, G.; Su, L.; Xiong, R.; Hong, S. Crustal deformation on the northeastern margin of the Tibetan plateau from continuous GPS observations. *Remote Sens.* **2019**, *11*, 34. [CrossRef]
50. Zheng, W.; Zhang, P.; Wu, C.; Li, Z.; Ge, W.; Wang, W.; Wang, Y. basic characteristics of active tectonics and associated geodynamic processes in continental china. *J. Geomech.* **2019**, *25*, 699–721. (In Chinese with an English abstract)
51. Cacciola, M.; Pellicanò, D.; Megali, G.; Lay-Ekuakille, A.; Versaci, M.; Morabito, F.C. Aspects about air pollution prediction on urban environment. In Proceedings of the 4th IMEKO TC19 Symposium on Environmental Instrumentation and Measurements 2013: Protection Environment, Climate Changes and Pollution Control, Lecce, Italy, 3–4 June 2013; International Measurement Confederation (IMEKO): Budapest, Hungary, 2013; pp. 15–20.
52. Shen, Z.K.; Jackson, D.D.; Kagan, Y.Y. Implications of geodetic strain rate for future earthquakes, with a five-year forecast of M5 earthquakes in Southern California. *Seismol. Res. Lett.* **2007**, *78*, 116–120. [CrossRef]
53. Segall, P. *Earthquake and Volcano Deformation*; Princeton University Press: Princeton, NJ, USA, 2010.

54. Bird, P.; Kreemer, C.; Holt, W.E. A long-term forecast of shallow seismicity based on the Global Strain Rate Map. *Seismol. Res. Lett.* **2010**, *81*, 184–194. [CrossRef]
55. Bird, P.; Kreemer, C. Revised tectonic forecast of global shallow seismicity based on version 2.1 of the Global Strain Rate Map. *Bull. Seismol. Soc. Am.* **2015**, *105*, 152–166. [CrossRef]
56. Doglioni, C.; Barba, S.; Carminati, E.; Riguzzi, F. Role of the brittle-ductile transition on fault activation. *Phys. Earth Planet. Inter.* **2011**, *184*, 160–171. [CrossRef]
57. Riguzzi, F.; Crespi, M.; Devoti, R.; Doglioni, C.; Pietrantonio, G.; Pisani, A.R. Geodetic strain rate and earthquake size: New clues for seismic hazard studies. *Phys. Earth Planet. Inter.* **2012**, *206*, 67–75. [CrossRef]
58. Guo, Z.; Qin, B.; Xu, W.; Tang, Q. Preliminary study on a model for the development of the focus of an earthquake. *Acta Geophys. Sin.* **1973**, *16*, 43–48. (In Chinese with an English abstract)
59. Zhu, S.; Zhang, P. Numeric Modeling of the Strain Accumulation and Release of the 2008 Wenchuan, Sichuan, China, EarthquakeNumeric Modeling of the Strain Accumulation and Release of the 2008 Wenchuan, China, Earthquake. *Bull. Seismol. Soc. Am.* **2010**, *100*, 2825–2839. [CrossRef]
60. Zhu, S.; Zhang, P. FEM simulation of interseismic and coseismic deformation associated with the 2008 Wenchuan Earthquake. *Tectonophysics* **2013**, *584*, 64–80. [CrossRef]
61. Dong, S.; Zhang, P.; Zheng, W.; Yu, Z.; Lei, Q.; Yang, H.; Jinfeng, L.; Gong, H. Paleoseismic observations along the Langshan range-front fault, Hetao Basin, China: Tectonic and seismic implications. *Tectonophysics* **2018**, *730*, 63–80. [CrossRef]
62. Xu, X.; Deng, Q. The features of late quaternary activity of the piedmont fault of Mt. Huoshan, Shanxi Province and 1303 Hongdong earthquake (Ms = 8). *Seismol. Geol.* **1990**, *12*, 21–32, (In Chinese with an English abstract)